UNIFORMED SERVICES UNIVERSITY OF THE HEALTH SCIENCES
4301 JONES BRIDGE ROAD
BETHESDA, MARYLAND 20814-4799

18 JUNE 2003

APPROVAL SHEET

Title of Thesis: " Digital Mammography Breast Dosimetry Using Copper-Doped Lithium Fluoride (LiF:MCP) Thermoluminescent Dosimeters (TLDs)"

Name of Candidate: LT John J. Tomon
Master of Science in Public Health
Department of Preventive Medicine and Biometrics

Thesis and Abstract Approval:

_____	_____
Chairman: Thomas E. Johnson, PhD.	Date
_____	_____
Research Advisor: CDR David A. Schauer, ScD.	Date
_____	_____
Lt Col Kristin N. Swenson, PhD.	Date
_____	_____
Col David J. Louis, MD., MS.	Date
_____	_____
Lt Col Peter T. LaPuma, PhD.	Date

Report Documentation Page

Form Approved
OMB No. 0704-0188

1. REPORT DATE	2. REPORT TYPE	3. DATES COVERED
2003	**N/A**	**-**

4. TITLE AND SUBTITLE
Digital Mammography Breast Dosimetry Using Copper-Doped Lithium Fluoride (LiF:MCP) Thermoluminescent Dosimeters (TLDs)

5a. CONTRACT NUMBER
5b. GRANT NUMBER
5c. PROGRAM ELEMENT NUMBER

6. AUTHOR(S)
LT JOHN J. TOMON

5d. PROJECT NUMBER
5e. TASK NUMBER
5f. WORK UNIT NUMBER

7. PERFORMING ORGANIZATION NAME(S) AND ADDRESS(ES)
Uniformed Services University of the Health Sciences

8. PERFORMING ORGANIZATION REPORT NUMBER

9. SPONSORING/MONITORING AGENCY NAME(S) AND ADDRESS(ES)

10. SPONSOR/MONITOR'S ACRONYM(S)
11. SPONSOR/MONITOR'S REPORT NUMBER(S)

12. DISTRIBUTION/AVAILABILITY STATEMENT
Approved for public release, distribution unlimited

13. SUPPLEMENTARY NOTES

14. ABSTRACT

The determination of mean glandular dose (MGD) to the breast is an essential aspect of mammography equipment evaluations and exposure controls. The American College of Radiology (ACR) Quality Control Manual outlines the procedure for MGD determination in screen-film mammography based upon conversions of entrance skin exposures (ESEs) measured with an ionization chamber (IC). The use of digital mammography has increased because of the need for improved object resolution and tissue contrast. Digital mammography incorporates a different image receptor (solid-state detector), which may lead to different MGDs compared to screen-film mammography. Therefore, evaluating and verifying the applicability of the ACRs MGD methodology to digital mammography is essential in determining the carcinogenic risk associated with digital mammograms. This research measured the applicability and accuracy of the ACRs MGD methodology to digital mammography. MGD measurements were determined using the light output from TLD-100H (LiF:MCP) TLDs and conversions of ESEs measured with an IC (ACR methodology). The statistical evaluation of the MGD data revealed the ACRs MGD methodology is not applicable to the imaging modality of digital mammography (all P values <0.05). The comparison of the TLD and IC MGD calculations resulted in a measured MGD differential no greater than 0.12 mGy. Additionally, a more rigorous method of MGD was calculated by averaging the thermoluminescent (TL) absorbed dose at various depths throughout a breast phantom. This more through method of calculating MGD resulted in a MGD of 1.34 mGy ± 0.07 mGy as compared to the ACRs methodology MGD of 1.34 mGy ± 0.001 mGy. These results coupled with the narrow precision of both the TL and IC measurements supports the conclusion that the ACR methodology for MGD determination does apply to the modality of digital mammography. Backscatter measurements from the image receptors of both mammography modalities statistically show there is a difference (all P values <0.001) in the radiation backscattered from each image receptor.

15. SUBJECT TERMS

16. SECURITY CLASSIFICATION OF:			17. LIMITATION OF ABSTRACT	18. NUMBER OF PAGES	19a. NAME OF RESPONSIBLE PERSON
a. REPORT **unclassified**	b. ABSTRACT **unclassified**	c. THIS PAGE **unclassified**	**SAR**	**60**	

Standard Form 298 (Rev. 8-98)
Prescribed by ANSI Std Z39-18

The author hereby certifies that the use of any copyrighted material in the thesis manuscript entitled:

Digital Mammography Breast Dosimetry Using Copper-Doped Lithium Fluoride (LiF:MCP) Thermoluminescent Dosimeters (TLDs)

beyond brief excerpts is with the permission of the copyright owner, and will save and hold harmless the Uniformed Services University of the Health Sciences from any damage, which may arise from such copyright violations.

John J. Tomon
LT, MSC, USN
Department of Preventive Medicine and Biometrics
Uniformed Services University of the Health Sciences

ABSTRACT

Title of Thesis: "Digital Mammography Breast Dosimetry Using Copper-Doped Lithium Fluoride (LiF:MCP) Thermoluminescent Dosimeters (TLDs)"

Author: LT John J. Tomon
Master of Science in Public Health

Thesis Directed by: CDR David A. Schauer
Assistant Professor of Radiology/Radiological Sciences
Department of Radiology

The determination of mean glandular dose (MGD) to the breast is an essential aspect of mammography equipment evaluations and exposure controls. The American College of Radiology (ACR) Quality Control Manual outlines the procedure for MGD determination in screen-film mammography based upon conversions of entrance skin exposures (ESEs) measured with an ionization chamber (IC). The use of digital mammography has increased because of the need for improved object resolution and tissue contrast. Digital mammography incorporates a different image receptor (solid-state detector), which may lead to different MGDs compared to screen-film mammography. Therefore, evaluating and verifying the applicability of the ACR's MGD methodology to digital mammography is essential in determining the carcinogenic risk associated with digital mammograms. This research measured the applicability and accuracy of

the ACR's MGD methodology to digital mammography. MGD measurements were determined using the light output from TLD-100H (LiF:MCP) TLDs and conversions of ESEs measured with an IC (ACR methodology). The statistical evaluation of the MGD data revealed the ACR's MGD methodology is not applicable to the imaging modality of digital mammography (all P values <0.05). The comparison of the TLD and IC MGD calculations resulted in a measured MGD differential no greater than 0.12 mGy. Additionally, a more rigorous method of MGD was calculated by averaging the thermoluminescent (TL) absorbed dose at various depths throughout a breast phantom. This more through method of calculating MGD resulted in a MGD of 1.34 mGy ± 0.07 mGy as compared to the ACR's methodology MGD of 1.34 mGy ± 0.001 mGy. These results coupled with the narrow precision of both the TL and IC measurements supports the conclusion that the ACR methodology for MGD determination does apply to the modality of digital mammography. Backscatter measurements from the image receptors of both mammography modalities statistically show there is a difference (all P values <0.001) in the radiation backscattered from each image receptor.

Digital Mammography Breast Dosimetry Using Copper-Doped Lithium Fluoride (LiF:MCP) Thermoluminescent Dosimeters (TLDs)

BY

LT JOHN J. TOMON

Thesis submitted to the Faculty of the Department of Preventive Medicine and Biometrics and the Department of Radiology/Radiological Sciences Graduate Program of the Uniformed Services University of the Health Sciences in partial fulfillment of the requirement for the Degree of Master of Sciences in Public Health, 2003

ACKNOWLEDGEMENT

I am grateful to the Department of Radiology at the National Naval Medical Center (NNMC), especially CDR(sel) Michelle F. Loscocco, for providing the support needed to complete this work.

I am grateful to the Ionizing Radiation Division of the National Institute of Standards (NIST), especially Mr. Stephen M. Seltzer, Mrs. C. Michelle O'Brien, and Dr. Christopher G. Soares, for providing their in-depth knowledge and guidance in the area of personnel dosimetry.

I would like to thank Capt (ret.) Jerry A. Thomas and Dr. Alexander Romanyuhka for the use of their laboratory facilities and their knowledge and expertise in the field of mammography. I want to thank all the members of my committee for their time and assistance in helping me complete this program. I especially want to thank Dr. Thomas E. Johnson and CDR David A. Schauer for inspiring this research idea and encouraging me to keep charging, even when I saw no light at the end of the tunnel.

DEDICATION

To my wife, Kelly, and my son Travis for the sacrifices you have made during my twenty-year Naval career and the last two years of study. Both of you are my strength, love and inspiration and I dedicate this thesis to both of you.

To mother and father, Dorothy and George Wassum, thank you both for the moral and spiritual compass you instilled in me early in life.

TABLE OF CONTENTS

LIST OF TABLES

LIST OF FIGURES

CHAPTER ONE: INTRODUCTION

Background and Significance

According to the American Cancer Society, breast cancer is the second leading cause of cancer death for women in the United States. Early detection and diagnosis is an essential key in the treatment and survivability of breast cancer. Mammography requires the highest quality of imaging techniques and fine detail over a wide spectrum of object contrasts in order to successful identify cancerous growths in their earliest stages of development (Byng, *et al*. 1998). The female breast is a radiosensitive organ (Dance, 1990) in which cancer usually originates in glandular breast tissues (Ng, *et al.,* 1997). Glandular tissues, including the acinar and ductal epithelium and associated stroma, are the most radiosensitive and susceptible to carcinogenesis (Dance, 1990). Ensuring the highest quality of breast tissue contrast and object resolution represents one of the most serious challenges of breast tissue imaging.

Mammography, more specifically standard screen-film mammography, has long been the primary methodology for breast cancer detection and diagnosis. In fact, mammography is generally thought of as the most accurate and reliable method for detecting minimal non-palpable breast cancer (Ng, *et al.,* 1997). However, breast imaging and cancer detection is not without some risk due to the ionizing radiation (x-ray) exposure to the patient's breast. The Food and Drug Administration (FDA), American College of Radiology (ACR) and Mammography Quality Standards Act (MQSA) have established limits of 3.0

mGy for MGD in order to minimize the risk to the glandular tissue (Gentry, *et al.*, 1996).

A determination of mean glandular dose (MGD) delivered to breast tissue is typically calculated using procedures and published tables from Section II of the ACR's Mammography Quality Control Manual (ACR, 1999). These published tables are based on factors such as entrance skin exposure (ESE), x-ray tube anode material used (Molybdenum (Mo) or Rhodium (Rh)), beam quality (half-value layer, HVL) breast thickness, and the composition of the breast tissue (Wu, *et al.,* 1991). These FDA approved procedures are accepted as the standard dosimetric methodology for MGD determination in screen-film mammography. However, with the increased demand to achieve improved tissue contrast resolution and greater object resolution, screen-film mammography is being replaced by digital mammography. Digital mammography incorporates different detection hardware (solid state image receptor) and methods, which may lead to different MGDs compared to screen-film mammography. Therefore, evaluating and verifying the ACR's methodology for calculating MGD in digital mammography is essential in minimizing the risk to glandular tissues from digital mammograms.

Statement of the Problem

The determination of MGD to the breast is an essential part of mammography equipment evaluations and exposure controls. The approved ACR methodology for MGD determination entails a direct measurement of

collisional air Kerma (Ka) and its conversion to absorbed dose through the use of calculated conversion factors (Wu, *et al.,* 1991). This methodology is the standard used for MGD determination and is based upon the conventional screen-film image receptor used in mammography. Digital mammography uses a solid-state detector (Amorphous Silicon with Cesium Iodide (CsI)) as its image receptor. This difference in image receptor could result in differences in radiation backscatter and ultimately MGD measurements. In order to verify the applicability of the ACR's MGD methodology to digital mammography, MGD measurements were performed using thermoluminescent (TL) material (LiF:MCP) and ionization chamber (IC) measurements.

Research Goal

The goal of this research was to determine if the currently accepted ACR methodology for MGD determination is applicable to the breast imaging modality of digital mammography. Also, the results of this research will help to determine if there is a difference in radiation backscattered from the image receptor of standard screen-film to that of digital mammography. These differences could result in over/under estimates of MGD, and ultimately to risk estimates that are used in conjunction with digital mammography. Finally, the methods used in this research will help to determine the effects of varying breast tissue by measuring the light output of the TL material at various depths in the tissue compositions.

Research Question and Specific Aims

Research Question: Is the ACR methodology for MGD determination in screen-film mammography applicable to the imaging modality of digital mammography?

Specific Aims:

1. Measure MGD from a digital mammography machine in a custom made breast phantom of 50% adipose tissue and 50% glandular tissue using a National Institute of Standards and Technology (NIST) traceable TL dosimetry system. Measurements are made for selected clinical beam codes and results are compared to the ACR MGD ionization chamber data using standard statistical methods.
2. Determine the effect of varying tissue compositions on breast dose by measuring depth dose profiles in a digital mammography machine using LiF:MCP TLDs in the following breast phantoms:
    a. 100% glandular tissue
    b. 50% glandular and 50% adipose tissue
    c. 100% adipose tissue.
3. Measure a depth dose profile in a screen-film mammography machine using LiF:MCP TLDs in the 50% glandular and 50% adipose tissue breast phantom.

CHAPTER TWO: LITERATURE REVIEW

Mean Glandular Dose (MGD)

MGD is a universal term used in the field of diagnostic breast imaging that provides a means of characterizing the carcinogenic risk associated with diagnostic mammograms (Ng, *et al.,* 1997). This term represents the average absorbed radiation dose to the most radiosensitive tissues (glandular tissues) of the female breast. (Ng, *et al.,* 1997 and Wu, *et al.,* 1991). The MGD to the female breast from diagnostic mammograms is contingent on properties and qualities of both the x-ray beam and the breast tissue itself. The two most important characteristics of the breast tissue are the thickness of the breast and the tissue composition of the breast (Hammerstein, *et al.,* 1979). Glandular breast tissues are more susceptible to radiation-induced carcinogenesis then adipose and skin tissues. Additionally, it takes more x-ray exposure to penetrate denser (glandular) breast tissue then fatty (adipose) breast tissue and more exposure to penetrate a thicker breast than a thinner breast (Stanton, *et al.,* 1984). The characteristics of the x-ray beam also influence the absorbed dose to breast tissue. The x-ray beam characteristics that are of particular importance to MGD determination are the beam quality (half-value layer (HVL)) and the target material (anode) of the x-ray tube. The HVL is the indirect measure of the energies of the photons from the x-ray beam and is determined by the amount of material required to reduce the x-ray beam intensity by 50% (Bushberg, *et al.,* 2002). Both of these properties are important in the determination of MGD,

because both influence the energy spectrum of the photons in the mammography beam.

Calculation and Determination of MGD

The traditional and approved method of determining MGD is by measuring the ESE and converting it to MGD. The ESE measurements are performed using an IC placed next to a 4.2 cm 50% adipose/50% glandular phantom (ACR, 1999). These measurements require off central axis free in air measurements of ESE and use of conversion tables developed by Wu, *et al.* (ACR, 1999 and Ng, *et al.,* 1997). The conversion tables in the ACR's MQSA manual include the following factors: the x-ray tube's voltage in kVp, target and filter combination and the HVL of the beam (ACR, 1999). The table values convert the air exposure measured in Roetgens (R) to absorbed dose in units of millirad (mrad) and is expressed in equation 1 (Ng, *et al.,* 1997).

$$D_g = D_{gN} * X_{ESE} \qquad \text{Eq. 1}$$

The term D_g represents the MGD, D_{gN} is the normalized average glandular dose per ESE (conversion factors) and X_{ESE} is the measured ESE. The conversion factors (D_{gN}) are based on Monte Carlo calculations of the predominant photon-tissue interactions in mammography (Wu, *et al.,* 1991). The specific photon-tissue interactions of interest in mammography are the photoelectric effect, incoherent scattering and coherent scattering (Wu, *et al.,* 1991). This calculated MGD represents the average dose to the most radiosensitive breast tissues (glandular tissue) and describes the carcinogenic risk associated with ionizing radiation exposure from mammography (Ng, *et al.,* 1997).

Mammography (Digital vs. Screen-Film)

Mammography units are special radiographic x-ray machines that are specifically designed to image the female breast. The units consist of the standard components found in a general radiographic x-ray machine with some selective changes that are necessary to image the softer tissues found in the female breast. The important differences between the general radiographic machines and mammography units involve the target (anode) material and filters used. The most common target materials in use in mammography units are Mo, with the availability to change target material to Rh and Tungsten (W). The typical x-ray beam filtration in mammographic machines include some form of inherent filtration such as Beryllium (Be) and the capability to select additional filtration materials such as Mo and Rh. The versatility of mammography machines to be adjusted to select target, filtration combinations and tube voltages (kVp) allows for optimized image quality.

However, the most important aspects of the mammography unit involve the image receptor used to record the image. The most common type of image receptor used is screen-film mammography with digital mammography gaining wider acceptance. The screen-film units use single emulsion films with a special cassette. These cassettes contain a low attenuation carbon fiber with a Terbium-activated Gadolinium Oxysulfide (Gd_2O_2S: Tb) phosphor screen (Bushberg, *et al.*, 2002). The cassette and film combination are designed to ensure the best spatial resolution of the image. This is accomplished by placing the film on top of the phosphor screen, which allows the x-rays to pass through

the top of the cassette and film before interacting with the phosphor screen (Bushberg, *et al.*, 2002). Digital mammography units employ a completely different type of image receptor than screen-film units. The image receptor used in digital mammography units is an amorphous silicon array with a cesium iodide (CsI) solid-state detector. In this detector, the x-rays are absorbed by the CsI scintillator and converted to light photons (540 nm wavelength). The light photons emitted from the CsI scintillator are absorbed by the photodiodes in the amorphous silicon array and converted to an electronic charge. The photodiodes represent picture elements (pixels) of the image and their electronic charge output is sent to an image processor for viewing (Figure 1).

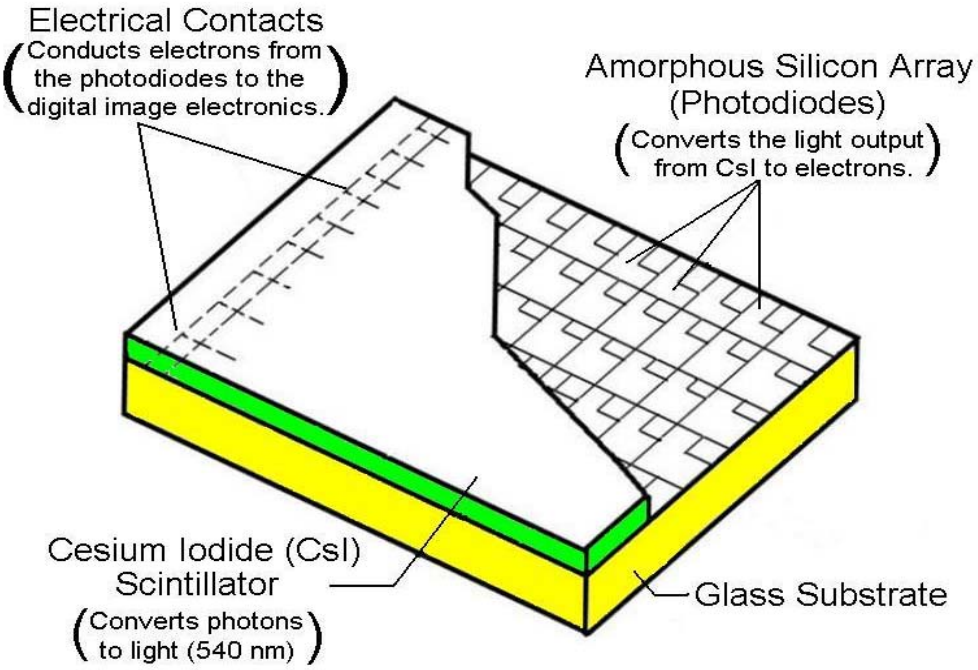

Figure 1: Digital Mammography Image Receptor

TLD-100H LiF (Mg, Cu, P) Dosimeters

The principle of thermoluminescence involves the controlled emission of light from certain materials (crystals) after exposure to ionizing radiation (McKeveer, *et al*., 1995). The electrons in the structure of the crystal are normally tightly bound in the valence band at room temperature. However, after being exposed to ionizing radiation these electrons gain sufficient energy to leave the valence band and create an electron-hole pair (Figure 2). These electrons and holes are then captured in impurities in the crystal structure (called activators) at energy levels below the conduction band in the forbidden energy gap. These electron-hole pairs remain trapped in a meta-stable state until acted upon by an external source of energy. When sufficient external energy is provided to the crystal in the form of heat, the electron-hole pairs recombine and return to the valence band, which results in the emission of energy in the form of light (Figure 2).

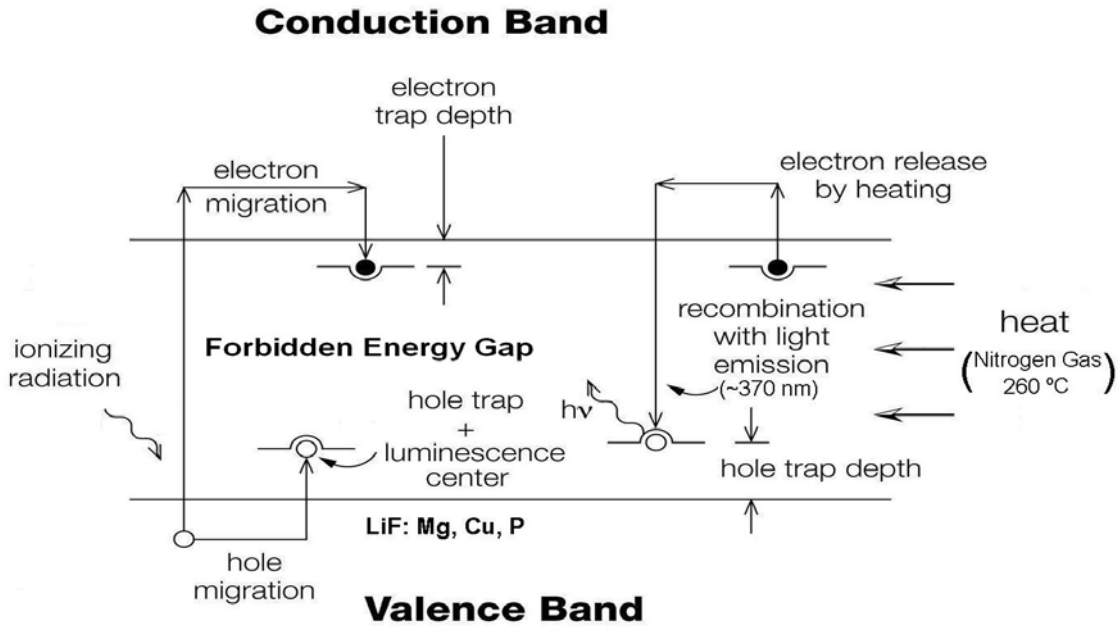

Figure 2: Thermoluminescence Phenomena

The light output of the TL material is a function of the recombination of the electron-hole pairs created by the ionizing radiation and can be related to the energy deposited by the ionizing radiation. Since the traps created by the activators exist at differing energy levels, the light output of the TL material will vary as a result of the heating temperatures and result in a function called a glow curve (Figure 3).

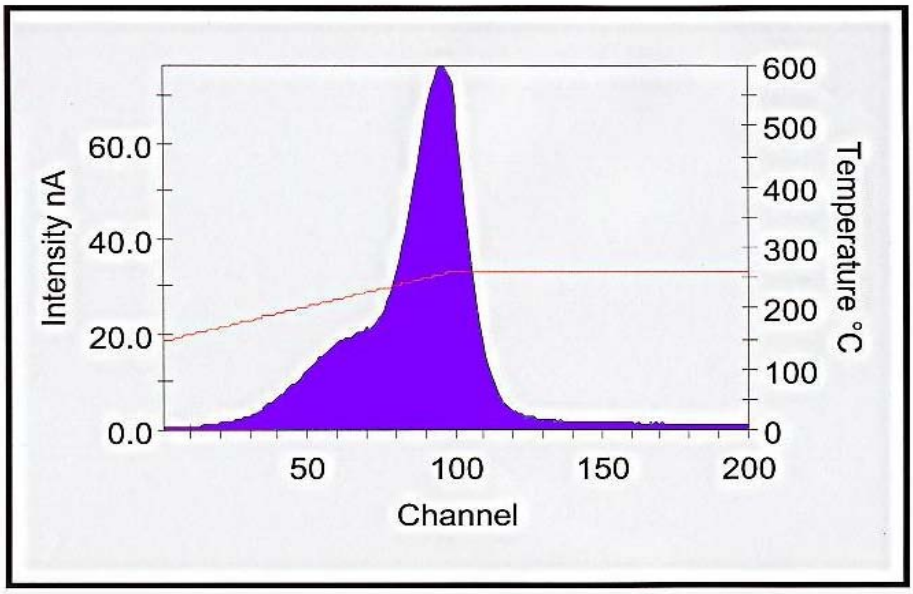

Figure 3: TLD-100H Glow Curve

TLD-100H (LiF:MCP) dosimeters are a highly sensitive type of thermoluminescence material that is composed of a Lithium (Li) Fluoride (F) crystal structure with Magnesium (Mg), Copper (Cu) and Phosphorous (P) impurities. The Mg impurities play a role in the electron-hole pair trapping action of the crystalline structure, while the P is related to recombination sites in the crystal (McKeveer, *et al*., 1995). The Cu seems to play a role at both the trapping sites and recombination sites; however, the precise TL characteristics of

this material are unknown (Chen, *et al.*, 2002). The combination of this TL material and associated impurities gives this dosimeter an effective atomic number (Z_{eff}) of approximately 8.14 (McKeveer, *et al*., 1995). When Z_{eff} of LiF:MCP is compared to that of soft tissue ($Z_{eff} \approx 7.4$) it is clearly evident that these dosimeters are relatively tissue equivalent, which is an important attribute when incident photon radiation is in the region of diagnostic radiology (few tens of keV) (Miljanic, *et al.*, 2002). Other highly attractive characteristics of LiF:MCP dosimeters are it's improved signal to noise ratio and less energy dependence than LiF:Mg, Ti (titanium) dosimeters, no measurable fading for periods of up to two months at room temperature or during high humidity conditions and no supralinear behavior with dose (McKeever, *et al*., 1995, Chen, *et al*., 2002 and Miljanic, *et al*., 2002). The main disadvantage of the TLD-100H (LiF:MCP) dosimeter is the loss of the dosimeter's sensitivity when heated to temperatures greater than 270ºC (Chen, *et al*., 2002).

CHAPTER THREE: MATERIALS AND METHODS

Breast Phantom:

Description and Construction

Computerized Imaging Reference Systems (CIRS), Inc. of Norfolk Virginia, fabricated the phantoms used in this research according to the specifications of the Uniformed Services University of the Health Sciences (USUHS) Mammography Research Team. The breast phantoms are constructed in semi-circular slabs of material that vary in thickness and elemental composition (Figure 4). The elemental composition of each type of breast phantom was designed to approximate the various types of female breast tissues. The breast phantoms range from extremely dense breast tissue (100% glandular), to a moderately dense breast tissue (50% glandular/ 50% adipose) to minimally dense breast tissue (100% adipose). The breast phantoms are fabricated from plastic water epoxy resin and Table 1 shows the percent elemental composition and tissue density of each type. The plastic water resin materials are formulated to maximize breast tissue simulation properties at typical mammography x-ray energies of 20 keV. The phantoms

Figure 4: Breast Phantom

Breast Phantom Type	Elemental Composition						Physical Density (g cm^{-3})
	H	C	N	O	Cl	Ca	
100% Adipose	0.098	0.714	0.020	0.164	0.002	0.001	0.94
50/50	0.096	0.703	0.019	0.170	0.002	0.009	0.99
100% Glandular	0.094	0.691	0.018	0.177	0.001	0.018	1.05

Table 1: Phantom Characterization (Data provided by CIRS Inc.)

can be varied in thickness by placing the 1.0 cm, 0.5 cm and 0.2 cm slabs of the phantom material together to construct a simulated compressed breast of different sizes. All of the phantoms used in this research are 4.2 cm thick, which is the thickness of the breast phantom currently used to perform MGD measurements (ACR, 1999). Additionally, the design of these breast phantoms incorporates a separate 1.0 cm slab of each type of phantom material that is capable of housing 26 TLD-100H (3.60 mm dia. x 0.38 mm thick) dosimeters (Figure 5). This specific 1.0 cm slab allowed for the measurement of dose at the surface of the phantom, at depths of 1.2 cm and 2.2 cm in the phantom and the exit dose from the phantom (image receptor backscatter).

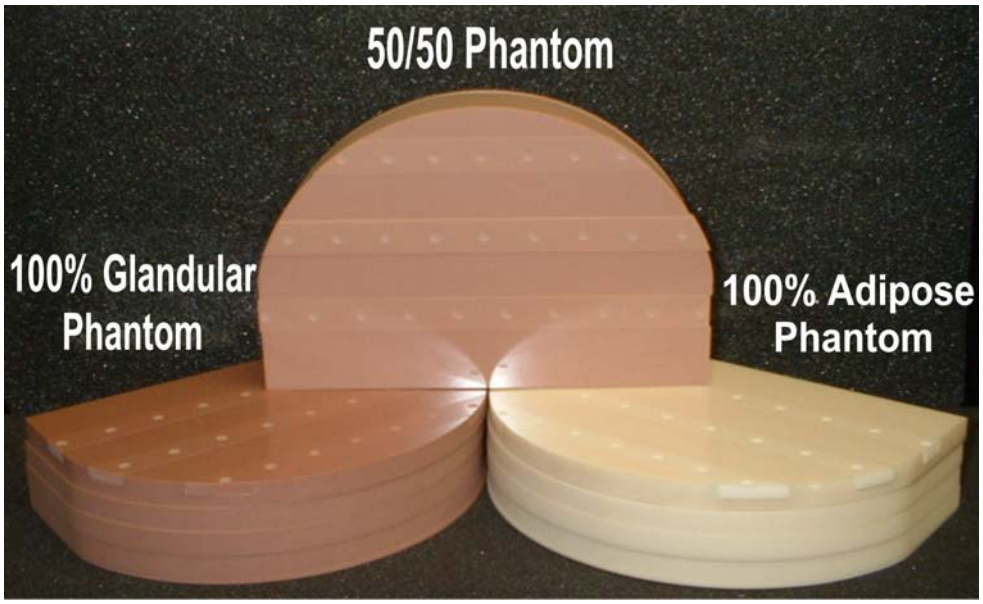

Figure 5: Breast Phantoms with TLD-100H Inserts

Radiological Characterization

A radiological characterization of the phantom material is required to determine how well it corresponds to breast tissue. The interactions of the mammographic x-rays in the different phantom materials are key to understanding how much energy is deposited in the phantom. The mass-energy absorption coefficients [$\mu_{en}(E)/\rho$] for the three phantom compositions were obtained from calculations performed by Mr. Seltzer (Seltzer, 1993) of NIST. The calculated values then were ratioed to International Commission on Radiation Units and Measurements (ICRU) Report 44 mass-energy absorption coefficients for air. Figure 6 shows that at the mammographic x-ray energy of 20 keV, the ratio of mass-energy absorption coefficients of the 100% glandular phantom to air most closely approximates the ratio of ICRU soft tissue to air.

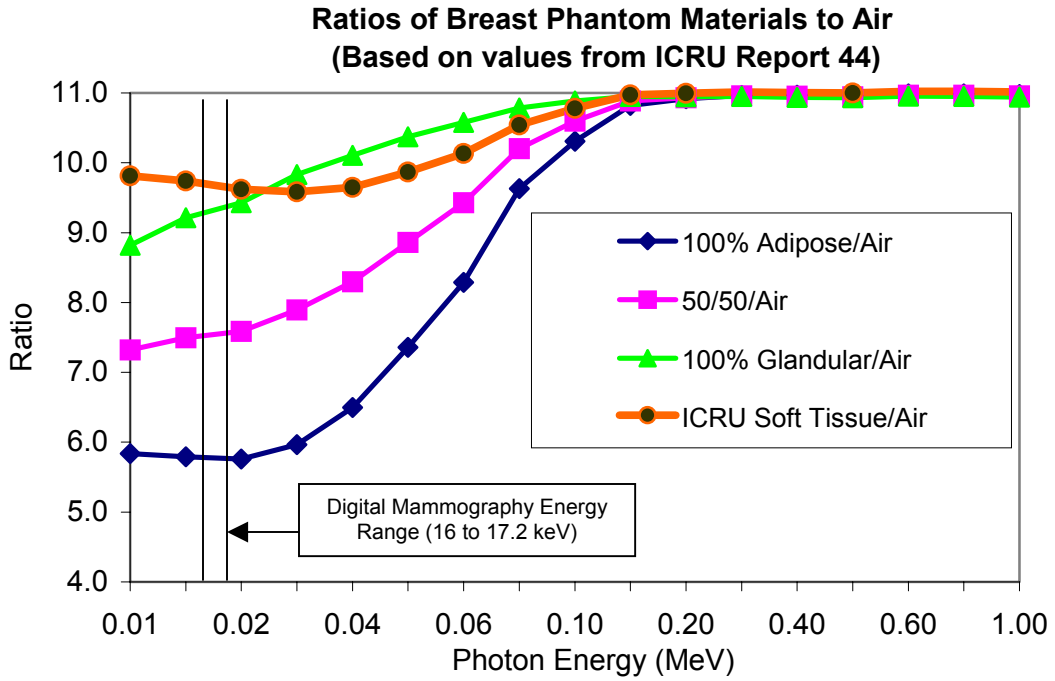

Figure 6: Ratios of Mass-Energy Absorption Coefficients for Three Breast Phantom Compositions to Air as a Function of Photon Energy

Additionally, the ratios of mass-energy absorption ratios for 50/50 and 100% adipose phantoms are less than that of soft tissue to air.

The next part of the characterization of the phantoms involved the calculation of *f*-factors as a function of energy and then as a function of depth for the three different phantom materials. The energy spectrum used to generate these factors was based on the Institute of Physics and Engineering in Medicine (IPEM) Catalogue of Diagnostic X-ray Spectra and other data. *F*-factors for any medium can be determined using equation 2.

$$f_{med} = \frac{\int \left[\mu_{en}(E)/\rho\right]_{med} E\, \Phi_o(E)\, dE}{\int \left[\mu_{en}(E)/\rho\right]_{air} E\, \Phi_o(E)\, dE} \qquad \text{Eq. 2}$$

Where $[\mu_{en}(E)/\rho]$ is the mass-energy absorption coefficient ($cm^2\ g^{-1}$) for both the phantom materials and air and $\Phi_o(E)$ is the fluence of photons of energy between E and E plus the bin width dE (Schauer, *et al.*,1993). To calculate the *f*-factor for a medium as a function of both energy and depth, the attenuation of the fluence at each depth must be taken into account using equation 3.

$$\Phi_d(E) = \Phi_o(E) e^{-\left(\frac{\mu(E)}{\rho}\right)(\rho)(d)} \qquad \text{Eq. 3}$$

Where $\Phi_o(E)$ is the fluence of photons of energy at depth zero, (d) is the depth (cm), $[\mu(E)/\rho]$ is the mass attenuation coefficient ($cm^2\ g^{-1}$) for the material and (ρ) is the physical density ($g\ cm^{-3}$) of the material (Attix, 1986). The mass attenuation coefficients $[\mu(E)/\rho]$ for the three phantom compositions and air were obtained from the NIST Photon Cross Section (X-COM) Database (Berger, *et al.*,

1998). The attenuated fluence at each depth $\Phi_d(E)$ can then be substituted for $\Phi_o(E)$ in equation 2 in order to obtain an *f*-factor at depth. The results of the *f*-factor calculations at depth for the different phantoms and mammography beam codes are listed in Table 2.

Breast Phantom Type	Phantom Depth (cm)	Mammography Beam Codes		
		Mo/Mo-28	Mo/Rh-28	Rh/Rh-30
100 % Adipose	0.0 (surface)	0.567	0.566	0. 568
100 % Adipose	1.2	0.171	0.197	0.171
100 % Adipose	2.2	0.079	0.096	0.079
100 % Adipose	4.2 (exit)	0.020	0.027	0.020
50/50	0.0 (surface)	0.731	0.734	0.731
50/50	1.2	0.169	0.200	0.169
50/50	2.2	0.066	0.085	0.067
50/50	4.2 (exit)	0.013	0.019	0.013
100% Glandular	0.0 (surface)	0.897	0.903	0. 897
100% Glandular	1.2	0.157	0.191	0.157
100% Glandular	2.2	0.052	0.070	0.053
100% Glandular	4.2 (exit)	0.007	0.012	0.008

Table 2: Breast Phantom *f*-factors for Three Clinically Relevant Mammography Beam Codes

TL Material and Processing System

The TL system used to process all TLD-100H (LiF: (MCP)) included the following components: the Bicron Model 5500 automatic TLD chip reader, a personnel computer (PC) with Windows NT and WINREMS software (ThermoElectron Corp., Solon, OH.) and Domnick Hunter Nitrox Compressor (Domnick Hunter Ltd., Charlotte, NC.) (Figure 7). The model 5500 automatic TLD reader is a PC operated instrument that is capable of processing 50 dosimeters at a time in a disc carrier. The 5500 reader is controlled by the

WINREMS software, which enables the operator the flexibility to calibrate the reader and dosimeters and control the processing parameters (Saint-Gobain, 2001).

Figure 7: TL System

The reader provides a dynamic range of reading over seven decades of light output (energy deposited) and can be used to process several different types of TL dosimeters. The PC drives the entire TL reader operation and along with the WINREMS software the operator can select the desired Time Temperature Profile (TTP). The TTP is an essential part of the operating parameters of the TL processing system and is key to the TL output data results. The TTP for this research is specific for the TLD-100H (LiF:MCP) and is shown in Figure 8. The use of pre-heat in this TTP is important to remove low temperature peaks that do not contribute useful information to the light output of the dosimeter. The proper TTP is essential to accurate and reliable output from the TLD-100H

(LiF:MCP) due to the loss of sensitivity of the TLD-100H material when heated above 270˚ C.

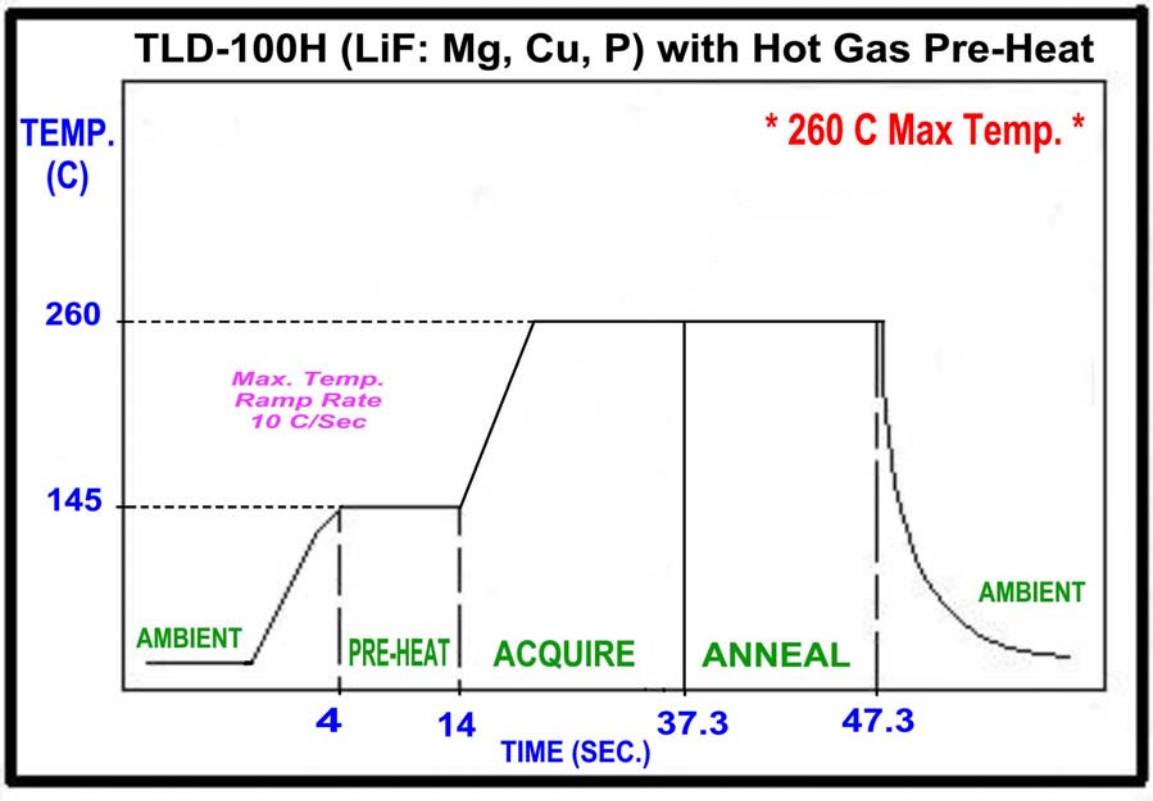

Figure 8: TLD-100H Time Temperature Profile With Hot Gas Pre-Heat

The last part of the TL processing system is the NITROX compressor, this unit provides high quality Nitrogen (N_2) gas for the heating of the TL material. The compressor provides 99.995% pure N_2 gas at a pressure of 40 to 90 psi with a flow rate of 400 L h^{-1}.

TL Material Characterization:

Population Determination of TL Material

Due normal variations in TLD-100H (LiF:MCP) dosimeter output response (≈ ±7.9%), the selection process for the TLDs started with the grouping of 400 TLD-100H (LiF:MCP) dosimeters into eight 50-disc batches. These individual

batches were then exposed to ionizing radiation from a Bicron Model 2210 TLD Irradiator. The irradiator contains 18 MBq (0.5 mCi) of $^{90}Sr/^{90}Y$ in secular equilibrium and is capable of uniformly irradiating the TLDs in the dosimeter carrier of the TLD reader. The TLDs were placed in the TLD reader and annealed by processing the dosimeters with a read cycle. The TTP used for this anneal cycle is listed in Table 3.

Parameter	Model 5500 (Hot gas with Pre-heat)
Preheat Temperature (˚C)	145
Preheat Time (sec)	10
Heating Rate (˚C sec^{-1})	10
Maximum Temperature (˚C)	260
Acquire Time (sec)	23 ⅓
Anneal Temperature (˚C)	260
Anneal time (sec)	10

Table 3: TTP for TLD-100H (LiF:MCP)

After the anneal cycle was completed, the batch was placed in the irradiator and exposed to approximately 108 mR (≈30 revolutions). The time between completion of the anneal cycle and irradiation was kept at a constant of five minutes for every batch. After completion of the irradiation cycle, the disc carrier and TLDs were placed in the TLD reader for the readout cycle. The time between the irradiation cycle and readout cycle was kept at a constant of five minutes for every batch. The light output response (nanoCoulomb (nC)) of each TLD was recorded for each of the 400 TLDs and then the mean light output and

standard deviation for the entire population were calculated. From this entire population of TLDs two sets were drawn for experimentation and for calibration. The criteria for the calibration set was to select the 15 TLDs with a sensitivity within ±1% and the criteria for the experimental set was to select the 150 TLDs with a sensitivity within ±3%. Table 4 shows the results of the population characterization of the TLD-100H (LiF:MCP) dosimeters with the sensitivity of the experimental set of ± 1.7% and the sensitivity of the calibration set of ± 0.14%.

	Entire LiF TLD Population	Experimental LiF TLDs	Calibration LiF TLDs
Population Size	400	150	15
Mean Light Output (nC)	66.19	66.18	66.14
Standard Deviation	1.91	0.67	0.07
Sensitivity (Range of Response)	± 7.9%	± 1.7%	± 0.14%

Table 4: TLD-100H (LiF:MCP) Population Data

Verification of TL Material Response Linearity

The next phase of the TL material characterization was a linearity check of the TLD-100H (LiF:MCP) dosimeters over a range of ionizing radiation exposures. This check was accomplished in two steps. The first step involved the computation of a reader calibration factor (RCF) using the calibration set of TLDs. The calibration set of TLDs was annealed using the procedure stated above and the TTP in Table 3. After the anneal cycle was completed, the batch was placed in the irradiator and exposed to ionizing radiation approximately 151.2 mR (≈42 revolutions). The time between completion of the anneal cycle

and irradiation was kept at a constant of five minutes. After completion of the irradiation cycle, the disc carrier and TLDs were placed in the TLD reader for the readout cycle. The time between the irradiation cycle and readout cycle was kept at a constant of five minutes. The light output response of each TLD was recorded for the calibration set of TLDs and then the mean light output and standard deviation for the set was calculated. The RCF of 0.615 (± 0.01) nC mR^{-1} was then calculated by using equation 4.

$$MGD = \frac{\text{mean light output}}{\text{exposure}} \qquad \text{Eq. 4}$$

The second step involved a check of the linearity of the light output response of both the experimental and calibration dosimeter sets. This check was performed by randomly separating the experimental and calibration sets of dosimeters into 15 batches each containing 11 dosimeters. Dosimeters were then placed in the disc carrier and annealed in the TLD reader. The TTP used for this anneal cycle is the same as listed in Table 3. After the anneal cycle was completed, the batch was placed in the irradiator and exposed to ionizing radiation ranging from 18 mR to 1000.8 mR. The time between completion of the anneal cycle and irradiation was kept at a constant of five minutes for every batch. After completion of the irradiation cycle, the TLDs were placed in the TLD reader for the readout cycle and the time between irradiation and readout was kept at a constant of five minutes for every batch. The light output response of each TLD was recorded for each batch of TLDs and then the mean light output and standard deviation for the batch were calculated. The observed dose (OD)

(mR) was calculated using equation 5 and then the ratio of OD to delivered dose (DD) was calculated with equation 6.

$$\text{Observed dose} = \left(\frac{\text{mean light output}}{\text{RCF}} \right) \qquad \text{Eq. 5}$$

$$\text{Ratio} = \left(\frac{\text{Observed Dose (OD)}}{\text{Delivered Dose (DD)}} \right) \qquad \text{Eq. 6}$$

Batch Number (n=11)	Mean Light Output (nC)	Standard Deviation (nC)	Observed Dose (OD) (mR)	Delivered Dose (DD) (mR)	Ratio (OD/DD)
1	11.9	0.21	19.4	18.0	1.08
2	31.6	0.55	51.3	50.4	1.02
3	62.1	1.04	101.0	100.8	1.00
4	92.6	1.50	150.5	151.2	0.99
5	122.8	2.39	199.7	201.6	0.99
6	155.3	3.01	252.4	252.0	1.00
7	186.6	3.70	303.3	302.4	1.00
8	218.0	3.57	354.4	352.8	1.00
9	248.5	3.84	404.0	403.2	1.00
10	275.4	4.52	447.8	450.0	0.99
11	309.2	5.49	502.8	500.4	1.01
12	388.2	4.14	631.2	626.4	1.01
13	459.7	11.27	747.4	752.4	0.99
14	541.3	9.17	880.2	874.8	1.01
15	618.6	12.21	1005.8	1000.8	1.01

Table 5: TLD-100H (LiF:MCP) Linearity Data

Table 5 shows the light output results from each batch and a comparison of the measured dose to the expected dose. Figure 9 represents a plot of the measured exposure to the expected dose for the 15 batches of TLDs. The results of the plot clearly indicate a linear response of both the calibration and experimental set of TLDs over the range of 18 mR to 1000.8 mR (R^2 = 0.999925).

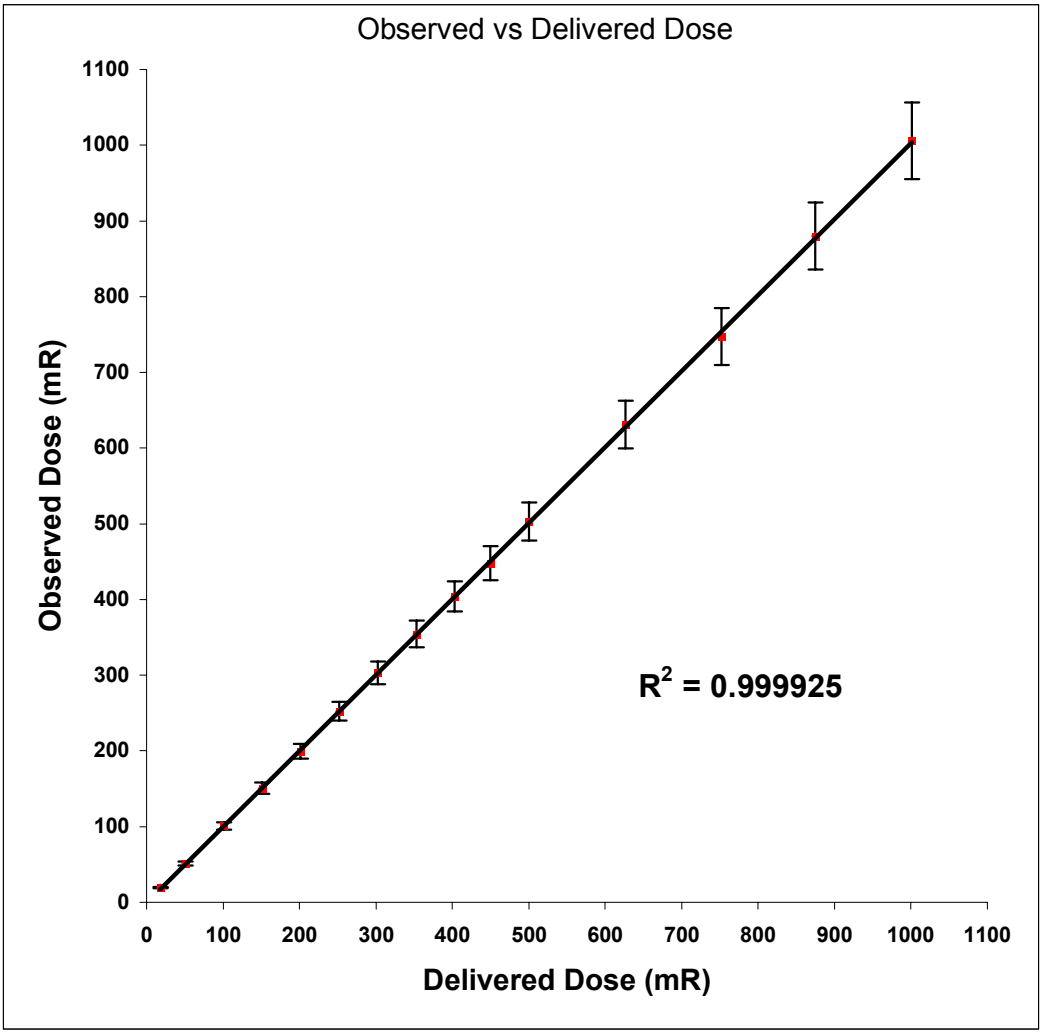

Figure 9: TLD-100H (LiF:MCP) Linearity Plot

NIST Traceable Calibration

The first work performed to establish a NIST traceable calibration of both the TLD-100H dosimeters and IC involved the identification and matching of the clinically relevant digital mammography beam codes to the available NIST mammography calibration range beam codes. This was accomplished by matching the beam codes from the applicable digital mammography technique chart used at National Naval Medical Center (NNMC) to the mammographic

beam codes available at the NIST mammography calibration range. The result of this investigation revealed three beam codes listed in Table 6.

Compressed breast thickness (mm)	100% Adipose Breast Tissue		
	kVp	mAs	Target/Filter
40-50	28	78	Mo/Rh
60-70	30	110	Rh/Rh
	50/50 Breast Tissue		
30-40	28	70	Mo/Mo
40-50	28	106	Mo/Rh
	100% Glandular Breast Tissue		
30-40	28	85	Mo/Mo

Table 6: Clinically Relevant Digital Mammography Beams

After selection of the three clinically relevant beams, the next step was determination of the uniformity of the NIST mammography calibration range beams. This was performed by placing radiographic films in the beams at a source-to-detector distance of 200 cm. The films were exposed to both the Mo and Rh targets at the NIST mammography range. After the films were developed the uniformity of the beams was determined using a scanning laser densitometer. The scanned film was then normalized to the center point of the film and the uniformity fields from both beams were determined to be within 6% at a field diameter of 12 cm. Figures 10 and 11 show the uniformity of the field for both target materials in the NIST mammography range. The calibration TLDs were placed within the 12 cm diameter of the 50/50 phantom and then irradiated in each of the mammography beams. The air kerma (K_a) delivered to the phantom and calibration TLDs was measured and used to calculate a NIST traceable calibration factor for the TLDs in units of nC mR^{-1}.

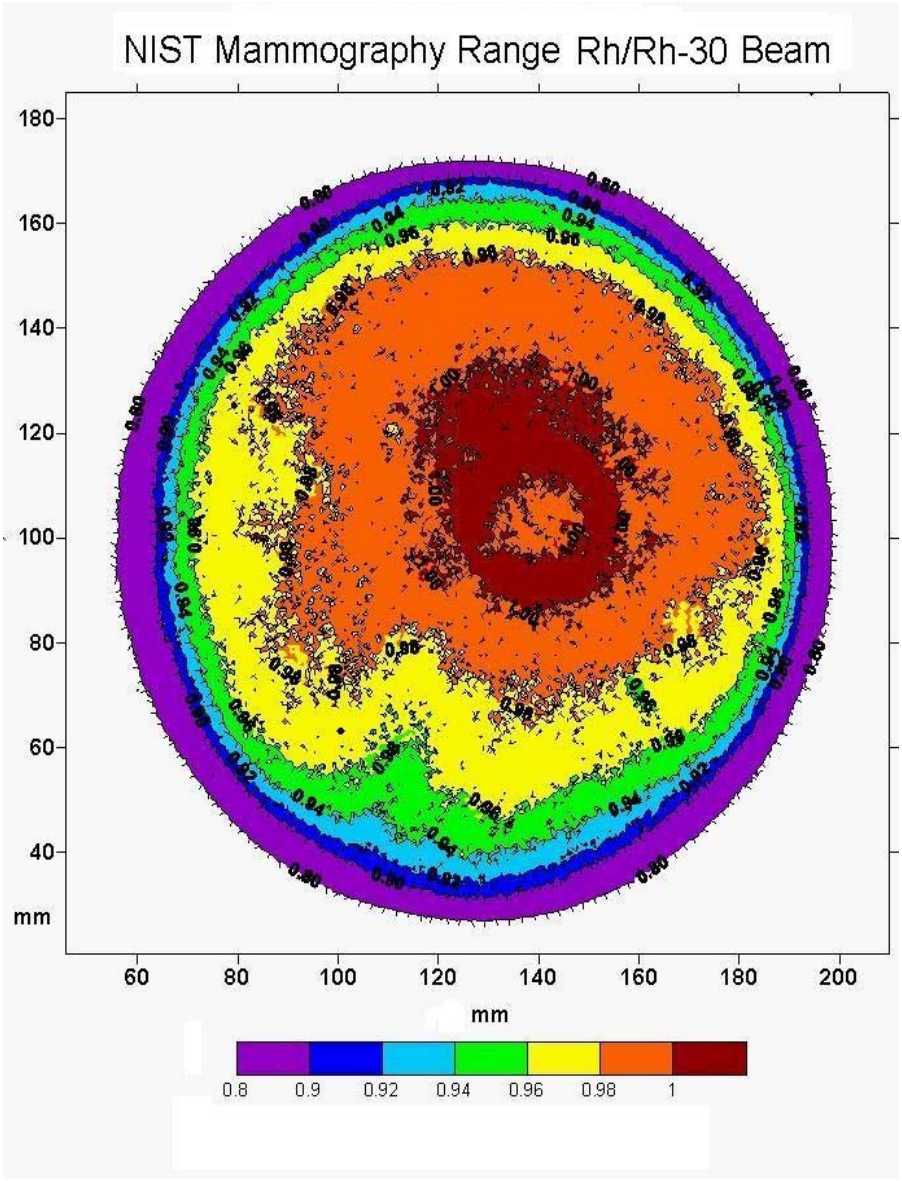

Figure 10: NIST Mammography Range Rh/Rh-30 Field Uniformity Film

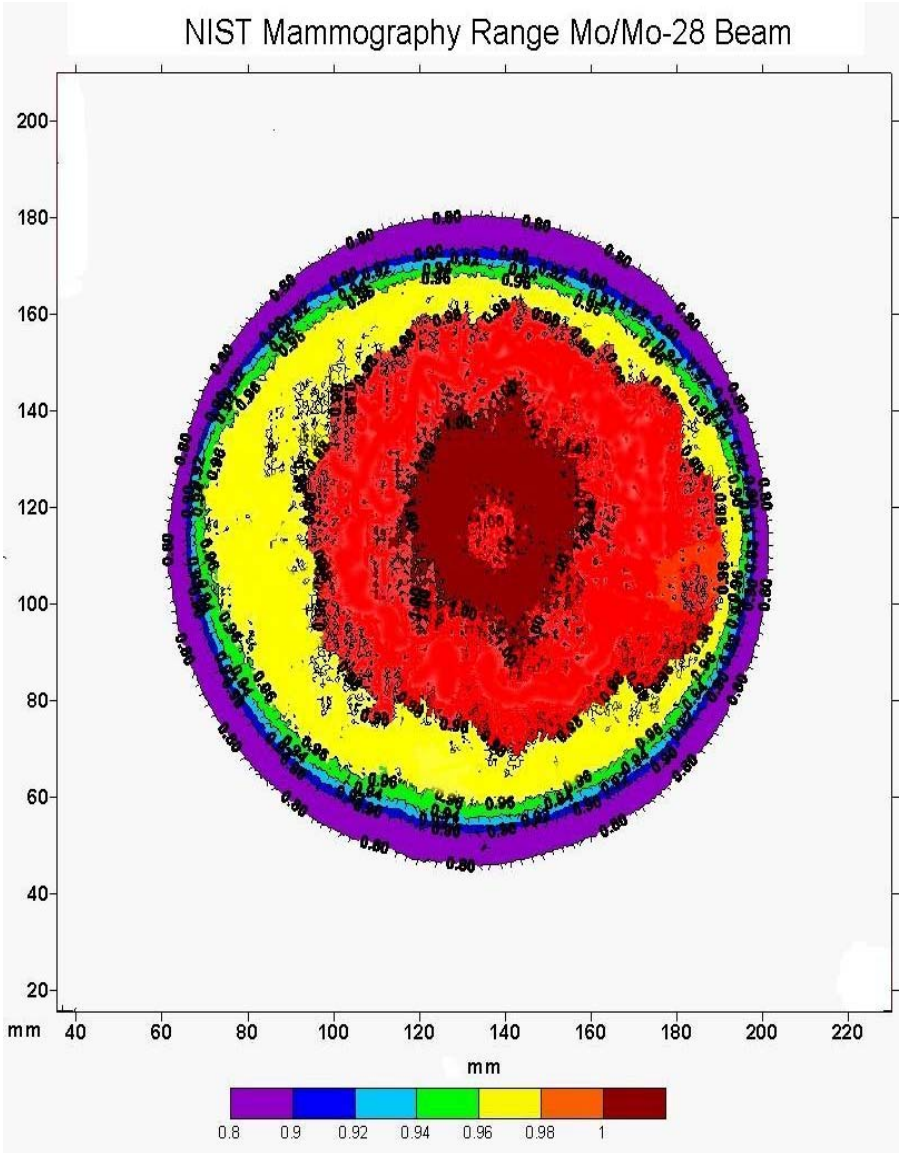

Figure 11: NIST Mammography Range Mo/Mo-28 Field Uniformity Film

The IC was calibrated using standard NIST calibration procedures (Lamperti, *et al.*, 2001) and the mammography beam codes of Table 6. Table 7 lists the NIST traceable calibration factors that were determined for both the IC and the LiF:MCP TLDs at the different mammography beam codes.

Mammography Beam Code	Ion Chamber Calibration Factor ($R\ C^{-1}$)	Mean TL Light Output (nC)	Exposure Delivered (mR)	TLD (LiF:MCP) Calibration Factor ($R\ C^{-1}$)
Mo/Mo-28	2.19×10^{8}	75.97	220.80	2.91×10^{6}
Mo/Rh-28	2.18×10^{8}	84.96	235.67	2.77×10^{6}
Rh/Rh-30	2.17×10^{8}	84.73	233.22	2.75×10^{6}

Table 7: NIST Traceable Calibration Factors.

MGD Measurements of Digital Mammography Unit

The MGD measurements experiments were designed to closely mimic the mammography quality control tests in the Medical Physicists section of the MQSA Manual (ACR, 1999). The first step of the experiment involved the determination of the beam quality HVL for each of the three-beam codes listed in Table 6. The setup of the digital mammography unit, IC and HVL measurements followed Procedure 9 of the Medical Physicist's section of the MQSA Manual (ACR, 1999). Equipment used in the experiment included a Keithley Triad Kit (Keithley Instruments, Cleveland, OH.) with a model 35050A dosimeter and model 96035B 15 cc IC and 0.1 mm-thick sheets of type 1145 aluminum alloy (99.9% pure Al). The results of the HVL measurements for the three-beam codes are listed in Table 8 along with the ACR's glandular dose conversion factors from Tables 1-3 of the MQSA Manual (ACR, 1999).

Target/Filter Combination	Tube Voltage (kVp)	HVL (mm Al)	Breast Phantom Type	ACR Conversion Factor (mrad/R)
Mo/Mo	28	0.36	50/50	183
Mo/Rh	28	0.40	50/50	204
Rh/Rh	30	0.43	50/50	232

Table 8. Calculated HVLs and ACR MGD Conversion Factors

The setup for the MGD measurements followed Procedure 10 in the Medical Physicist's section of the MQSA Manual (ACR, 1999) with the exception of the ACR's breast phantom. The ACR's breast phantom was substituted with a 4.2 cm thick 50/50 breast phantom shown in Figure 4. The breast phantom and IC were configured on the surface of the digital mammography image receptor as depicted in Figure 12. The 4.2 cm thick 50/50 breast phantom was oriented so the top slab of phantom material contained the inserts for the LiF:MCP TLDs.

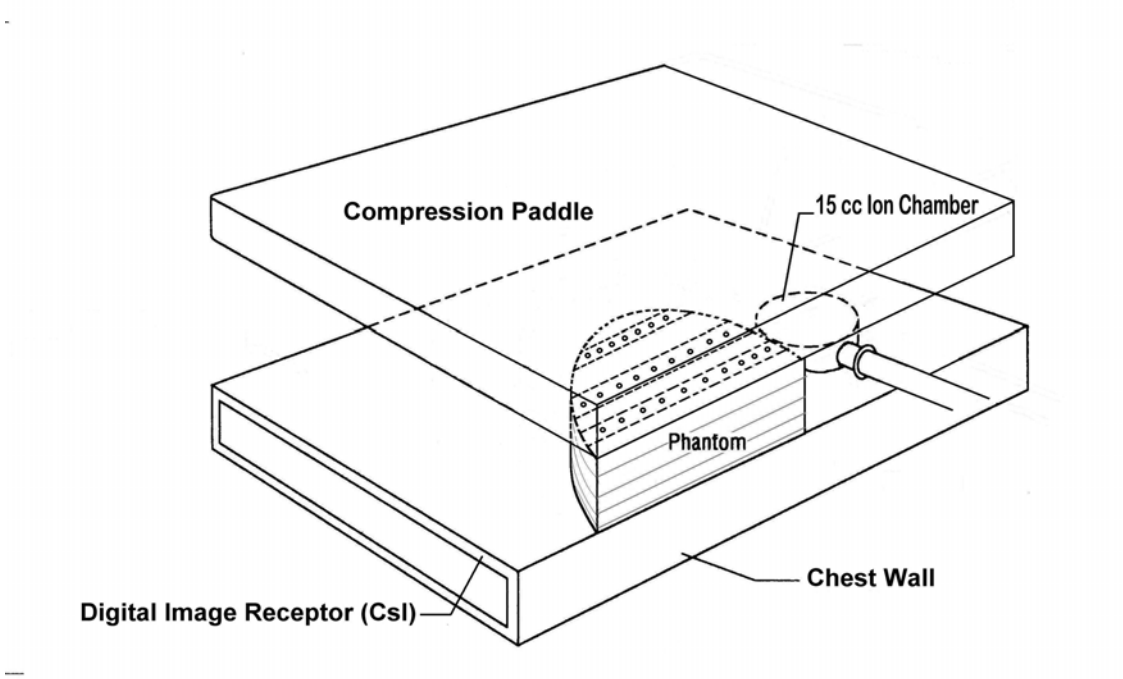

Figure 12. Experimental Geometry for MGD Measurements

Ten randomly selected TLDs from the experimental group were then placed in the three inserts on the surface of the phantom. The specific placement of the TLDs included four TLDs in the insert closest to the chest wall, four TLDs in the mid-breast insert and two TLDs in the insert closest to the nipple edge (see Figure 12). The compression paddle was then placed on top of the phantom with an applied compression pressure of 15 dekaNewtons (daN). The Senographe 2000 DMR (General Electric (GE) Medical Systems, Milwaukee, WI.) digital mammography unit was then setup for Mo/Mo target and filter combination, 28 kVp and 71 mAs. The phantom and IC were then irradiated and the meter reading of the IC recorded. The 10 TLDs were removed from the phantom and replaced position for position with another randomly selected 10 TLDs. The meter was reset and the experiment was repeated for a total of five separate irradiations.

The MGD experiment setup was repeated for both the Rh/Rh-30 and Mo/Rh-28 mammography beam codes. In each case, the ten randomly selected TLDs were placed in same locations in the inserts on the 50/50 breast phantom with the same compression pressure applied to the phantom for a total of five data runs for each beam code. Additionally, for each of the other mammography beam codes the digital mammography unit was configured for specific target and filter combinations, voltages and 71 mAs.

Depth Dose Measurements

The depth dose experiments were designed to measure the mean light output response of the LiF:MCP TLDs and the absorbed dose at various depths

in the breast phantoms. The setup for this experiment required the use of only one of the mammography beam codes listed in Table 6 and 4.2 cm thick breast phantoms of the three compositions listed in Table 1. The digital mammography unit was configured for a target and filter combination of Mo/Mo at 28 kVp and 71 mAs. The 4.2 cm thick 50/50 breast phantom was placed on top of the digital image receptor and oriented so that the top slab of phantom material contained the inserts for the LiF:MCP TLDs as shown in Figure 13. Twelve randomly selected TLDs from the experimental group were then placed in the three inserts on the surface of the phantom. The specific placement of the TLDs included four TLDs in the insert closest to the chest wall, five TLDs in the mid-breast insert and three TLDs in the insert closest to the nipple edge (see Figure 13). The compression paddle was then placed on top of the phantom with an applied compression pressure of 15 daN and the 50/50 breast phantom and twelve TLDs were irradiated. These twelve TLDs were then removed from the phantom and replaced with twelve different TLDs. The phantom was then re-configured so that slab of breast phantom material with the TLD inserts was now 1.2 cm below the surface of the breast phantom. The compression paddle was once again applied with a compression pressure of 15 daN and the breast phantom and TLDs were irradiated. This process was then repeated two additional times with TLDs placed at depths of 2.2 and 4.2 centimeters below the surface of the breast phantom. The measurement at the depth of 4.2 cm required the breast phantom to be turn upside down and be wrapped in 0.5 mm thick clear polyethylene to keep the TLDs from moving out of the inserts.

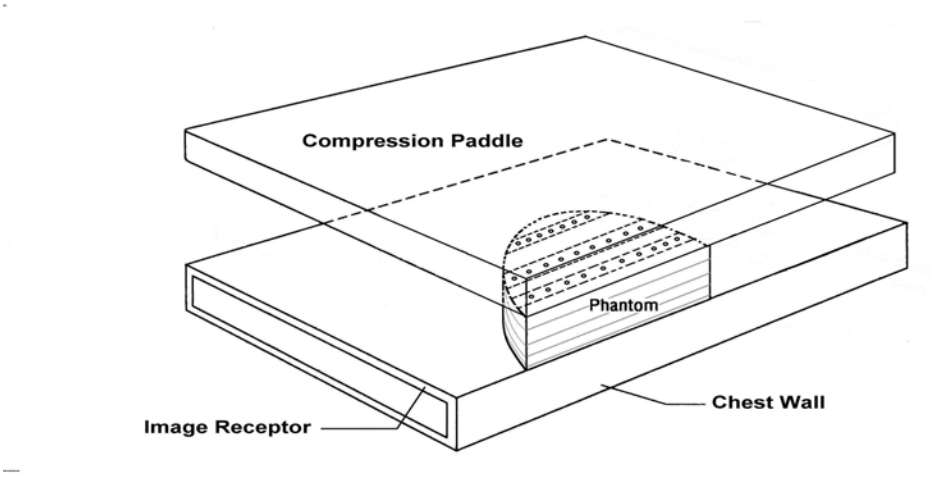

Figure 13. Experimental Geometry for Depth Dose Measurements

The depth dose experiment was then repeated for each of the 100% adipose and 100% glandular breast phantom using the same digital mammography machine settings, phantom configuration and depths.

The depth dose experiment was then repeated using the same thickness breast phantoms and TLD placement, but a screen-film mammography unit was used to irradiate the phantoms and TLDs. The screen-film mammography unit was a Senographe 2000 configured with the same target and filter combination, kVp and mAs that were used with the digital mammography unit. TLD placement for the screen-film mammography depth dose measurements was identical to the placement used in the digital mammography unit depth dose measurements.

CHAPTER FOUR: RESULTS AND DATA ANALYSIS

Analysis of MGD Data

The analysis of the MGD data resulted in a two-step process that involved the conversion of the LiF:MCP and IC raw data to MGD and then a statistical comparison of the two results. The data for the specific mammography beam codes were grouped into five paired samples. Each of the paired samples contained the average MGD from the ten LiF:MCP TLDs and the MGD from the associated IC reading. The LiF:MCP TLD data were statistically evaluated for normality by data run and phantom position for each of the mammography beam codes. Additionally the data were statistically evaluated to determine if there was a difference between the two methods for determining MGD.

The conversion of the LiF:MCP light output in nC to MGD in mGy involved the calculation of the average light output for each data run and conversion to MGD. The light outputs of the LiF:MCP TLDs were averaged for each data run, which resulted in five mean light output measurements in nC. These five mean light outputs were then converted to MGD (mGy) by using the beam-code specific ACR conversion factors (Table 8), NIST LiF:MCP calibration factors (Table 7) and equation 7. Table 9 lists the results of the LiF:MCP MGD (MGD_{TL}) calculations for each of the mammography beam codes tested.

$$\frac{\left(\begin{array}{c}\text{Mean Light}\\ \text{Output}\end{array}\right)\left(\begin{array}{c}\text{ACR Conversion}\\ \text{Factor}\end{array}\right)}{\left(\begin{array}{c}\text{NIST LiF : MCP}\\ \text{Calibratio n}\\ \text{Factor}\end{array}\right)}\left(0.01\,(\text{mGy mrad}^{-1})\right) = \text{MGD}_{\text{TL}} \quad \text{Eq. 7}$$

Data Run	Mo/Mo-28		Mo/Rh-28		Rh/Rh-30	
	Mean Light Output (nC)	MGD_{TL} (mGy)	Mean Light Output (nC)	MGD_{TL} (mGy)	Mean Light Output (nC)	MGD_{TL} (mGy)
1	260.50	1.39	238.08	1.35	322.45	2.06
2	261.07	1.39	235.95	1.33	319.27	2.04
3	261.39	1.39	233.22	1.32	320.25	2.05
4	260.96	1.39	234.49	1.33	317.12	2.03
5	261.44	1.39	234.70	1.33	317.79	2.03

Table 9: MGD_{TL} Results

The conversion of the IC exposure reading in R to MGD in mGy was a two-step process. The first step required the correction of the exposure reading to the NIST IC calibration factor ($R\ C^{-1}$) determined listed in Table 7. This correction factor (CF) was calculated for each of the mammography beam codes using the IC calibration factor programmed into the model 35050A dosimeter ($2.21 \times 10^8\ R\ C^{-1}$) and equation 8. Table 10 lists the CF for each mammography beam code.

$$\left(\frac{\text{NIST IC Calibration Factor } (R\,C^{-1})}{2.21 \times 10^{8}\ (R\,C^{-1})} \right) = CF \qquad \text{Eq. 8}$$

Mammography Beam Code	CF
Mo/Mo-28	0.99
Mo/Rh-28	0.99
Rh/Rh-30	0.98

Table 10: IC Correction Factors (CF)

The second step to converting the exposure reading involved the use of the CF calculated in equation 8, the ACR conversion factors (Table 8) and equation 9. Table 11 lists the results of the IC MGD (MGD_{IC}) calculations for each of the mammography beam codes tested.

$$(\text{Exposure})(\text{CF})\left(\begin{matrix}\text{ACR Conversion}\\ \text{Factor}\end{matrix}\right)\left(0.01\,(\text{mGy mrad}^{-1})\right)=\text{MGD}_{IC} \qquad \text{Eq. 9}$$

Data Run	Mo/Mo-28		Mo/Rh-28		Rh/Rh-30	
	Exposure (R)	MGD_{IC} (mGy)	Exposure (R)	MGD_{IC} (mGy)	Exposure (R)	MGD_{IC} (mGy)
1	0.736	1.34	0.648	1.31	0.849	1.94
2	0.737	1.34	0.648	1.31	0.848	1.94
3	0.737	1.34	0.647	1.31	0.846	1.93
4	0.736	1.34	0.646	1.31	0.846	1.93
5	0.737	1.34	0.646	1.31	0.846	1.93

Table 11: MGD_{IC} Results

The statistical evaluation of the MGD data required a determination of the distribution of the LiF:MCP TLD data and a comparison of the MGD_{TL} readings to the MGD_{IC} readings. The first test performed on the TLD data involved a check of the distribution of the light output data of the dosimeters. This was accomplished by looking at the distribution of TLD light output based on the TLD position in the phantom relative to the five data runs for each mammography beam code. As discussed in the MGD experimental design, the TLDs were placed in the same position for each of the data runs allowing the data to be grouped by the data run and phantom position. The standardized residuals for the TLD light output data were calculated and the normality of the distribution was tested using the statistical computer program Statistical Package for the Social Sciences (SPSS) 11.0 for Windows. The SPSS results of the distribution tests for normality are listed in Table 12 and Figures 14 -16 display the histograms for the distributions of the standardized residuals.

Standardized Residuals	Kolmogorov-Smirnov			Shapiro-Wilk		
	Statistic	df	Sig.	Statistic	df	Sig.
Mo/Mo-28$_{TL}$	0.11	50	0.20	0.95	50	0.03
Mo/Rh-28$_{TL}$	0.11	50	0.20	0.96	50	0.16
Rh/Rh-30$_{TL}$	0.11	50	0.19	0.96	50	0.10

Table 12: Normality Test Results (SPSS 11.0 for Windows)

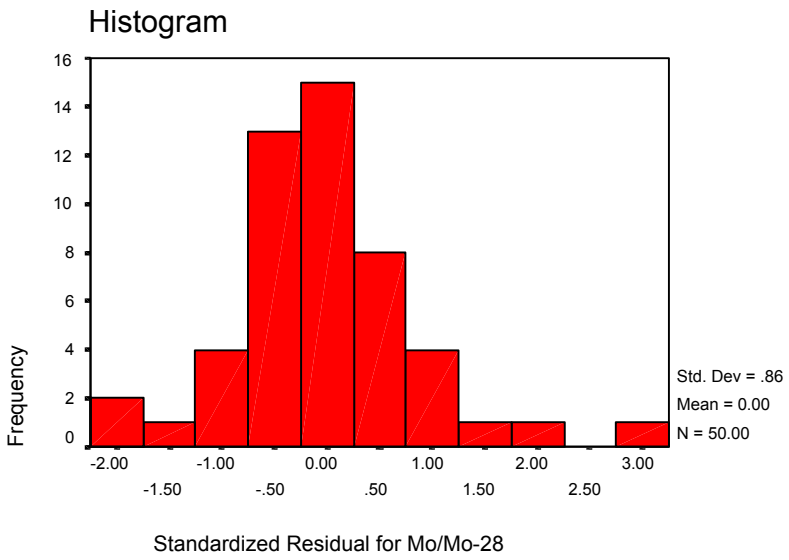

Figure 14: Standardized Residuals for Mo/Mo-28$_{TL}$

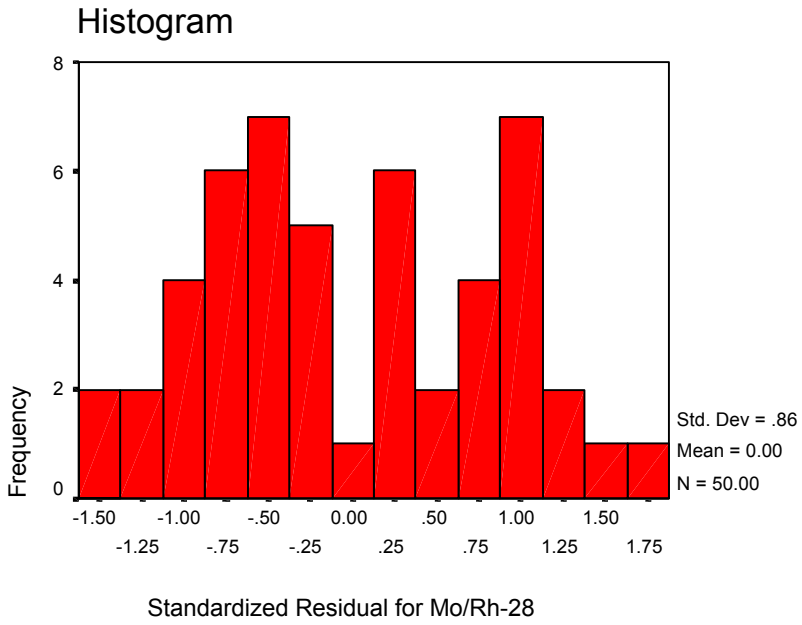

Figure 15: Standardized Residuals for Mo/Rh-28$_{TL}$

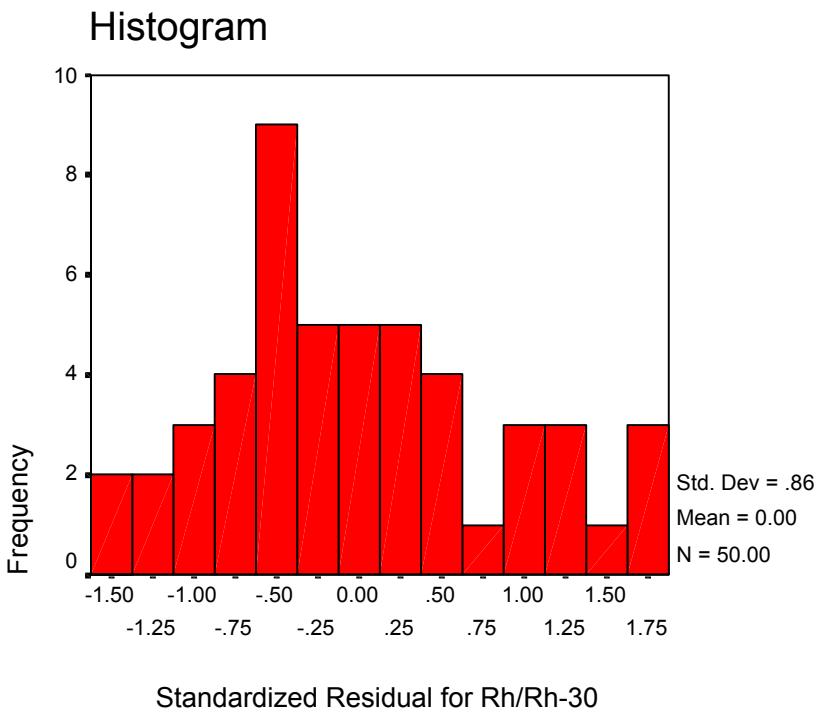

Figure 16: Standardized Residuals for Rh/Rh-30$_{TL}$

The second statistical test performed on the MGD data were the comparison of the MGD$_{TL}$ readings to the MGD$_{IC}$ readings. The MGD$_{TL}$ readings to the MGD$_{IC}$ readings were evaluated with a two-tailed Student's t-test and the statistical computer program SPSS 11.0 for Windows. The SPSS results of the paired sample statistics are listed in Table 13 and the results of the Student's t-tests are listed in Table 14.

Paired Data	Mean	N	Standard Deviation	Standard Error of the Mean
Mo/Mo-28 MGD$_{TL}$	1.39	5	0.002	0.0009
Mo/Mo-28 MGD$_{IC}$	1.34	5	0.001	0.0005
Mo/Rh-28 MGD$_{TL}$	1.33	5	0.010	0.0047
Mo/Rh-28 MGD$_{IC}$	1.31	5	0.002	0.0009
Rh/Rh-30 MGD$_{TL}$	2.04	5	0.013	0.0060
Rh/Rh-30 MGD$_{IC}$	1.93	5	0.003	0.0015

Table 13: MGD Paired Sample Statistics (SPSS 11.0 for Windows)

Paired Samples Test For MGD

		Paired Differences					t	df	Sig. (2-tailed)
		Mean	Std. Deviation	Std. Error Mean	95% Confidence Interval of the Difference				
					Lower	Upper			
Mo/Mo-28	MGD(TL) - MGD(IC)	.05080	.001304	.000583	.04918	.05242	87.1	4	.000
Mo/Rh-28	MGD(TL) - MGD(IC)	.0224	.00902	.00403	.0112	.0336	5.56	4	.005
Rh/Rh-30	MGD(TL) - MGD(IC)	.1080	.01125	.00503	.0940	.1220	21.5	4	.000

Table 14: MGD Paired Student's t-test Results (SPSS 11.0 for Windows)

Analysis of Depth Dose Profiles

The TLD light output data from the digital mammography and screen-film mammography depth dose experiments were evaluated and mean light output values were calculated at each depth in the breast phantoms. The mean light output and standard deviation of the TLDs at depth are listed in Tables 15 and 16. The mean light output at each depth was then normalized to the mean light output at the surface (0.0 cm) of the breast phantom.

Phantom Depth (cm)	50/50 Phantom		100% Adipose Phantom		100% Glandular Phantom	
	Mean Light Output (nC)	Standard Deviation (nC)	Mean Light Output (nC)	Standard Deviation (nC)	Mean Light Output (nC)	Standard Deviation (nC)
$0.0_{(surface)}$	262.8	10.4	269.3	12.6	254.8	12.7
1.2	90.4	4.8	114.5	5.5	69.8	3.3
2.2	42.2	2.2	62.0	3.5	28.5	1.2
$4.2_{(exit)}$	12.4	0.6	20.7	1.2	7.5	0.6

Table 15: Digital Mammography Depth Dose Measurements

Phantom Depth (cm)	50/50 Phantom		100% Adipose Phantom		100% Glandular Phantom	
	Mean Light Output (nC)	Standard Deviation (nC)	Mean Light Output (nC)	Standard Deviation (nC)	Mean Light Output (nC)	Standard Deviation (nC)
$0.0_{(surface)}$	254.2	13.3	256.0	15.2	243.1	12.7
1.2	86.5	5.9	110.7	7.0	66.3	3.9
2.2	40.1	2.1	59.2	3.6	26.5	1.4
$4.2_{(exit)}$	10.6	0.3	18.7	1.1	6.0	0.3

Table 16: Screen-Film Mammography Depth Dose Measurements

The normalized light output data for each breast phantom were then plotted as function of depth for both the digital and screen-film mammography units. Figures 17 and 18 are the plots of the normalized TL material light outputs.

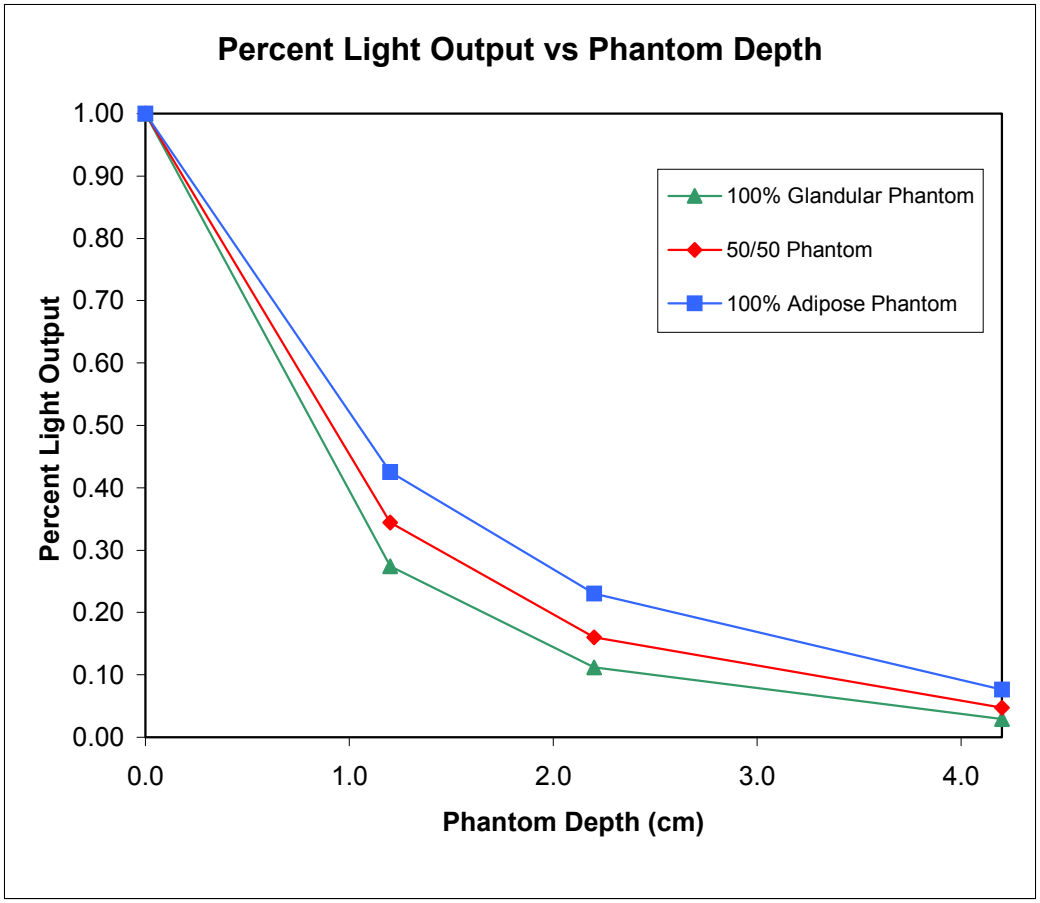

Figure 17: Digital Mammography Unit Graph of Light Output Versus Phantom Depth

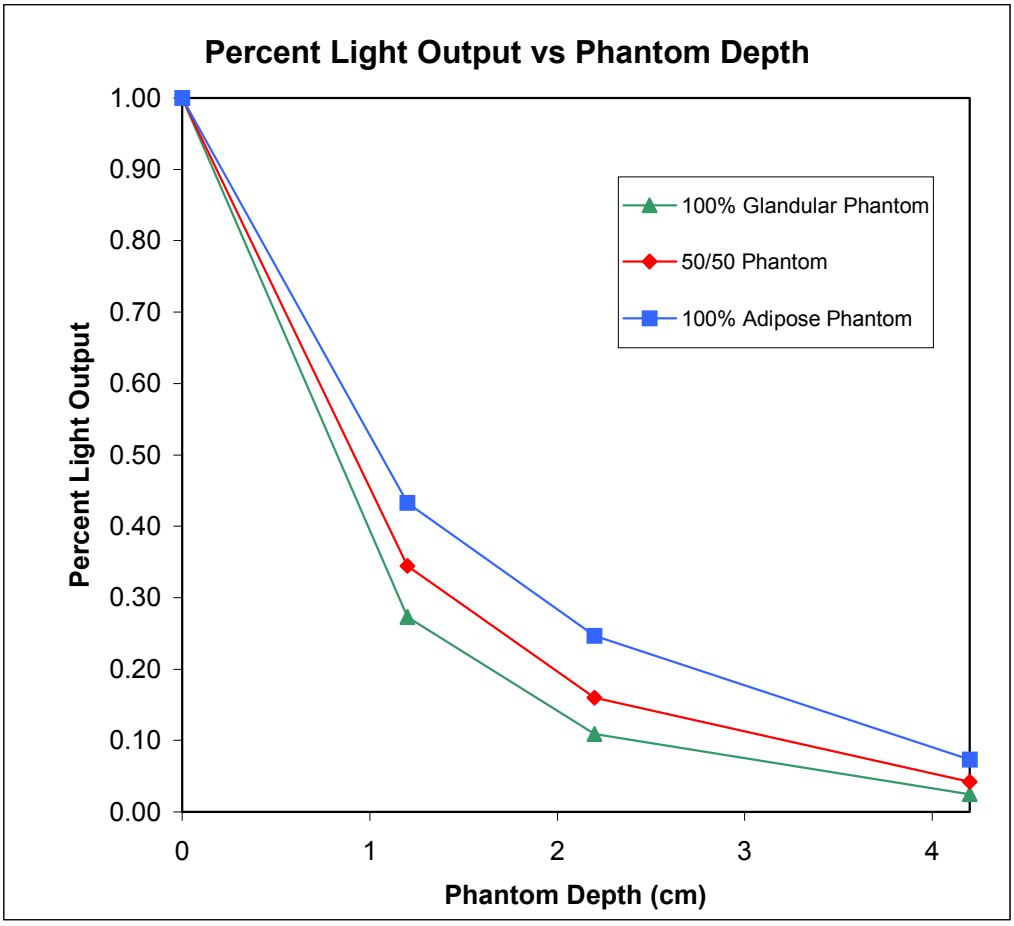

Figure 18: Screen-Film Mammography Unit Graph of Light Output Versus Phantom Depth

The TLD light output at the four depths in the 50/50 breast phantom were converted to absorbed dose and a depth dose profile for the 50/50 breast phantom was plotted. The absorbed dose at each depth in the phantom was calculated using the mean light output (Table 15), the 50/50 phantom depth *f*-factor (Table 2), the NIST LiF:MCP calibration factors (Table 7) and equation 10.

$$\frac{\left(\begin{array}{c}\text{Mean Light}\\ \text{Output}\end{array}\right)\left(\begin{array}{c}\text{50/50 Phantom}\\ f\text{ - Factor @ Depth}\end{array}\right)}{\left(\text{NIST LiF : MCP Calibration Factor}\right)}\left(\frac{\bar{w}}{e}\right)\left(0.01\,(\text{mGy mrad}^{-1})\right)=\text{MGD}_{\text{TL}} \qquad \text{Eq. 10}$$

The term $\left(\bar{w}/e\right)$ is 8.764 x 10^{-3} Gy R^{-1}, which converts exposure to absorbed dose at each of the depths in the 50/50 phantom. The results of these calculations along with the MGD are listed in Table 17.

Phantom Depth (cm)	Mean Light Output (nC)	Standard Deviation (nC)	Depth Dose (mGy)	Standard Deviation (mGy)
$0.0_{(surface)}$	262.8	10.4	4.897	0.19
1.2	90.4	4.8	0.389	0.02
2.2	42.2	2.2	0.071	4×10^{-3}
$4.2_{(exit)}$	12.4	0.6	0.004	2×10^{-4}
MGD (50/50 phantom *f*-factors)			1.34	0.07

Table 17: 50/50 Breast Phantom Depth Dose Values

The absorbed depth dose in the 50/50 breast phantom was fitted using Table Curve 2D (version 5.01) for Windows. Figure 19 shows the plot of the depth dose profile for the 50/50 breast phantom and the equation that mathematically describes this function.

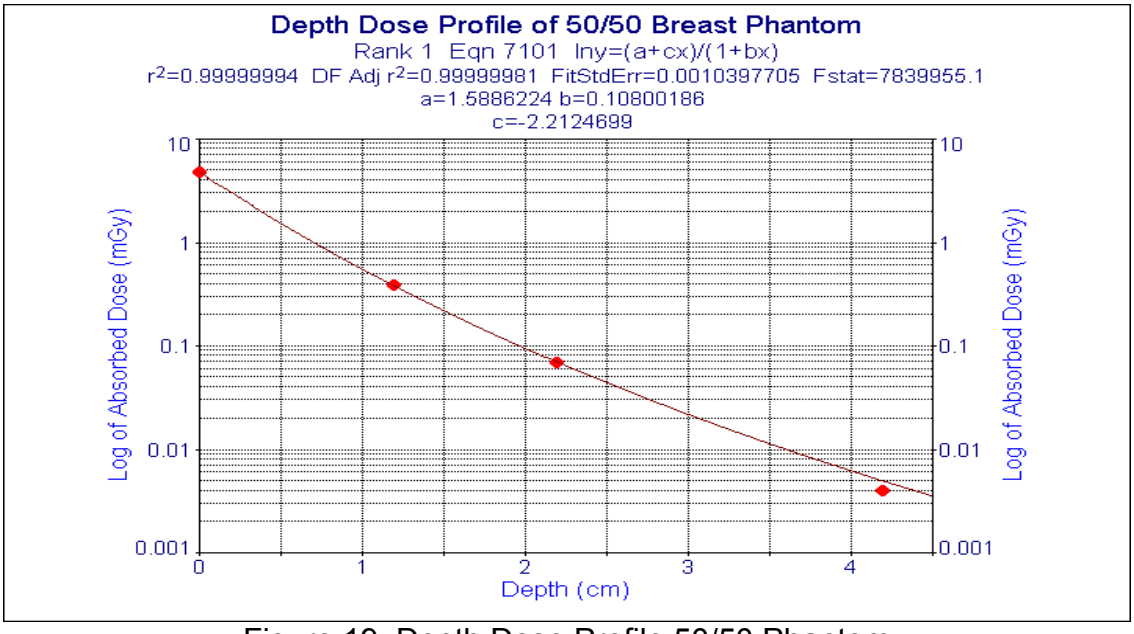

Figure 19: Depth Dose Profile 50/50 Phantom

Analysis of Backscatter Effects

The effects of image receptor backscatter were evaluated by analyzing the mean light output from the TLDs placed at the 0.0 cm phantom depth. The TLDs were placed in the same position in each breast phantom and the light output data from the TLDs were compared for each mammography unit. Since different mammography units were used to irradiate the TLDs in each phantom, the mean light outputs for each mammography unit was evaluated statistically using an independent sample two-tailed Student's t-test and the statistical computer program SPSS 11.0 for Windows. The SPSS results of the independent sample Student's t-test statistics are listed in Table 18 and the results of the independent sample Student's t-tests are listed in Table 19.

Group Data (Mo/Mo-28)	Mean (nC)	N	Standard Deviation (nC)	Standard Error of the Mean
Adipose $Phantom_{Screen\text{-}Film}$	18.7	12	1.13	0.33
Adipose $Phantom_{Digital}$	20.7	12	1.22	0.35
50/50 $Phantom_{Screen\text{-}Film}$	10.6	12	0.35	0.10
50/50 $Phantom_{Digital}$	12.4	12	0.62	0.18
Glandular $Phantom_{Screen\text{-}Film}$	6.0	12	0.31	0.09
Glandular $Phantom_{Digital}$	7.5	12	0.60	0.17

Table 18: Backscatter Group Sample Statistics (SPSS 11.0 for Windows)

Independent Samples Test Adipose Phantom (Mo/Mo-28)

		Levene's Test for Equality of Variances		t-test for Equality of Means						
		F	Sig.	t	df	Sig. (2-tailed)	Mean Difference	Std. Error Difference	95% Confidence Interval of the Difference	
									Lower	Upper
TLD Light Output (nC)	Equal variances assumed	.025	.876	-4.088	22	.000	-1.961	.480	-2.956	-.966
	Equal variances not assumed			-4.088	22	.000	-1.961	.480	-2.957	-.966

Independent Samples Test 50/50 Phantom (Mo/Mo-28)

		Levene's Test for Equality of Variances		t-test for Equality of Means						
		F	Sig.	t	df	Sig. (2-tailed)	Mean Difference	Std. Error Difference	95% Confidence Interval of the Difference	
									Lower	Upper
TLD Light Output (nC)	Equal variances assumed	1.343	.259	-8.72	22	.000	-1.796	.206	-2.223	-1.369
	Equal variances not assumed			-8.72	17	.000	-1.796	.206	-2.230	-1.362

Independent Samples Test Glandular Phantom (Mo/Mo-28)

		Levene's Test for Equality of Variances		t-test for Equality of Means						
		F	Sig.	t	df	Sig. (2-tailed)	Mean Difference	Std. Error Difference	95% Confidence Interval of the Difference	
									Lower	Upper
TLD Light Output (nC)	Equal variances assumed	4.121	.055	-7.83	22	.000	-1.528	.195	-1.933	-1.123
	Equal variances not assumed			-7.83	16	.000	-1.528	.195	-1.941	-1.115

Table 19: Backscatter Data Independent Sample Student's t-test Results (SPSS 11.0 for Windows)

CHAPTER FIVE: DISCUSSION AND CONCLUSIONS

Discussion

The light output data for the MGD experiments were tested for normality and graphically plotted on a histogram. The results from both normality tests performed on the Mo/Rh-28 and Rh/Rh-30 mammography beam codes indicate the mean light output data for these beam codes were normally distributed. The histograms for the Mo/Rh-28 and Rh/Rh-30 mammography beam codes graphically support both of the normality test results. The normality tests for the Mo/Mo-28 mammography beam indicated the light output data from these TLDs were not normally distributed. However, the histogram for the light output for the Mo/Mo-28 mammography beam depicted a normal distribution. Based on the results of the normality tests it was then assumed the light output data were normally distributed.

The MGD was determined using the TL material (MGD_{TL}) and the ACR's methodology involving IC measurements (MGD_{IC}). The data from each method of MGD determination were compared statistically using a Student's t-test. The Student's t-test was selected because of its robust nature to overcome minor violations in assumptions, such as the normal distribution of data and equality of variances. The paired Student's t-test was chosen because both the TLD and IC measurements in each data run were measured at the same time and were both subject to any random effects that would alter the measurement in the data run. The results of the paired Student's t-tests performed on the MGD measurements (Table 14) showed there is a statistically significant difference between means of

the MGD measurements (all P values <0.05). Additionally, the 95% confidence intervals for the paired Student's t-tests do not contain zero supporting the results of a statistically significant difference between the two means. The results of the MGD statistical tests supported rejection of the null hypothesis (H_o).

The backscatter effects of the image receptors for both the digital and screen-film mammography units were evaluated by comparing the light output of TLDs placed on the exit of the breast phantoms. The backscatter effects of the image receptors were tested statistically using an independent sample Student's t-test on the TLD light output from both the digital and screen-film mammography units. The independent sample Student's t-test was selected because random effects between each set of data could possibly vary at the time of measurement, thus making the data sets independent for each mammography unit. The results of the independent sample Student's t-tests (Table 19) revealed the variances of the data were equal and there is a statistically significant difference in TLD light output between the two image receptors (all P values <0.001). Additionally, the 95% confidence intervals for the independent sample Student's t-tests do not contain zero supporting the results of a statistically significant difference between the two means. The results of the image receptor backscatter statistical tests supported rejection of the null hypothesis (H_o).

Conclusions

When examined only in statistical context the results of this research do not support the hypothesis that the ACR's methodology for MGD determination is applicable to the modality of digital mammography. The statistical results

indicate there are statistically significant differences between the MGD_{TL} measurements and MGD_{IC} measurements. The statistical differences are most likely the results of the high degree of precision of the TLD system and IC used for these experiments, both of which resulted in small standard deviations. These precise instruments of measurement resulted in a MGD differential (between MGD_{TL} and MGD_{IC}) no greater than 0.12 mGy for each tested mammography beam code. Additionally, the MGD_{TL} was calculated for the Mo/Mo-28 mammography beam code and the 50/50 breast phantom by the more rigorous method of averaging the absorbed dose at four depths in the phantom. The result of this more thorough MGD_{TL} calculation (Table 17) is 1.34 mGy ± 0.07 mGy and is an exact match for the ACR's methodology (MGD_{IC}) of 1.34 mGy ± 0.001 mGy (Table 13). This result coupled with the narrow precision of both the TL and IC measurements supports the conclusion that the ACR methodology for MGD determination does apply to the modality of digital mammography.

APPENDIX A: LIMITATIONS

Limitations

The two limitations of this study involve the uncertainty of the data used to calculate the *f*-factors and design of the depth dose experiments. The fluence data used to calculate the *f*-factors were generated by Monte-Carlo calculations from the Institute of Physics and Engineering in Medicine (IPEM) Catalogue of Diagnostic X-ray Spectra and other data. The fluence data were neither specifically measured nor unfolded for these calculations; rather the IPEM catalogue used mammography machine parameters such as voltage, target and filter combinations and target angle to mathematically generate the x-ray fluence at the different energy levels. If the mammography fluence data were specifically measured and differences existed, then the calculated *f*-factors would change according to those measured differences.

The design of the depth dose experiments involved the use of only one of the three clinically relevant mammography beam codes (Mo/Mo-28) and three different phantom materials. The initial purpose of this experiment was to compare the effect of breast tissue composition and depth on TLD light output. This experiment allowed for the evaluation of light output at four different depths in the phantom and the more rigorous calculation of MGD_{TL} by averaging the absorbed dose at four depths in the phantom. However, due to this design the more rigorous method of MGD_{TL} calculation could not be calculated for the two additional mammography beams codes (Mo/Rh-28 and Rh/Rh-30) that were examined in the MGD_{TL} experiments. If additional the depth dose measurements

were performed on the 50/50 phantom in both the Mo/Rh-28 and Rh/Rh-30 mammography beams, then the calculated MGD_{TL} from the average absorbed depth dose in these beams could have been compared to the calculated MGD_{IC}. These calculations and comparisons would have provided additional data to support the conclusion that the ACR's methodology for MGD determination is applicable to the modality of digital mammography.

BIBLIOGRAPHY

American College of Radiology (1999) Mammography Quality Control Manual.

Attix, F. H., Introduction to Radiological Physics and Radiation Dosimetry, New York NY. US, John Wiley & Sons Publishing Inc.,(1986).

Berger, M. J., Hubbell, J. H., Seltzer, S. M., National Institute of Standards and Technology, Physics Laboratory, Ionizing Radiation Division, Photon Cross Section (XCOM) Database (1998)
http://physics.nist.gov/PhysRefData/Xcom/text/XCOM.html

Bushberg, J. T., Seibert, J. A., Leidholdt, E. M., Boone, J. M., The Essential Physics of Medical Imaging, Second Edition, Philadelphia PA. US, Lippincott Williams & Wilkins, 2002.

Byng, J. W., Mainprize, J. G., and Yaffe, M. J., X-ray Characterization of Breast Phantom Materials, Physics Medical Biology, 43 (1998) 1367-1377.

Chen, T. C., Stoebe, T. G., Role of Impurities in the Thermoluminescence of LiF:MG,Cu,P, Radiation Protection Dosimetry 100 (2002) 243-246.

Dance, D. R., Monte Carlo Calculation of Conversion factors for the Estimation of Mean Glandular Breast Dose, Physics Medical Biology, 35 (1990) 1211-1219.

Gentry, J. R., DeWard, L. A., TLD Measurements of *In-Vivo* Mammographic Exposures and the Calculated Mean Glandular Dose Across the United States, Medical Physics 23 (1996) 899-903.

Hammerstein, R. G., Miller, D. W., White, D. R., Masterson, M. E., Woodard, H. Q., Laughlin, J. S. Absorbed Radiation Dose in Mamography, Radiology 130 (1979) 485-491.

Lamperti, P. J., O'Brien, M., Calibration of X-Ray and Gamma-Ray Measuring Instruments, NIST Special Publication 250-58 (2001).

McKeever, S. W., Moscovitch, M., Townsend, P. D., Thermoluminescence Dosimetry Materials: Properties and Uses, Kent UK, Nuclear Technology Publishing, 1995.

Miljanic, S., Ranogajec-Komor, M., Knezevic, Z., Vekic, B., Main dosimetric Characteristics of Some Tissue–Equivalent TL Detectors, Radiation Protection Dosimetry 100 (2002) 437-442.

Ng, K. H., Aus, R. J., DeWerd, L. A., Vetter, J. R., Entrance skin Exposure and Mean Glandular Dose: Effect of Scatter and Field Gradient at Mammography, Radiology, 205 (1997) 395-398.

Schauer, D. A., Seltzer, S. M. and Links, J. M., Exposure-to-absorbed-dose Conversion for Human Adult Cortical Bone, Applied Radiation and Isotopes, 44 (1993) 485-489.

Saint-Gobain Ceramics and Plastics Inc. 2001 Model 550 Automatic TLD Reader with Win REMS Publication No. 5500-W-O-0901-003.

Seltzer, S. M., Calculation of Photon Mass Energy-Transfer and Mass Energy-Absorption Coefficients, Radiation Research, 136 (1993) 147-170.

Stanton, L., Villafana, T., Day, J. L., Lightfoot, D. A., Dosage Evaluation in Mammography, Radiology 150 (1984) 577-584.

Wu, X., Barnes, G. T., Tucker, D. M., Spectral Dependence of Glandular Tissue Dose in Screen-Film Mammography, Radiology, 179 (1991) 143-148.